The sulfur- and halogen-rich super eruption Los Chocoyos and its impacts on climate and environment

Hans Brenna[1], Steffen Kutterolf[2], Michael J. Mills[3], Kirstin Krüger[1]

[1]Section for Meteorology and Oceanography, Department of Geosciences, University of Oslo, P.O. Box 1022 Blindern,0315, Oslo, Norway.
[2]GEOMAR | Helmholtz Centre for Ocean Research Kiel, Wischhofstrasse 1-3, 24148, Kiel, Germany
[3]Atmospheric Chemistry Observations & Modeling Laboratory, National Center for Atmospheric Research, P.O. Box 3000, Boulder, Colorado 80307-3000, USA

Correspondence to: Kirstin Krüger (kkrueger@geo.uio.no)

Abstract. The super-eruption of Los Chocoyos, newly dated to 80.6 kyrs ago, in Guatemala was one of the largest volcanic events of the past 100,000 years. Recent petrologic data show that the eruption released very large amounts of climate-relevant sulfur and ozone destroying chlorine and bromine gases. Using the recently released Earth System Model CESM2(WACCM6) we simulate the impacts of the sulfur- and halogen-rich Los Chocoyos (~15° N) eruption on the pre-industrial Earth System for the eruption month January.

Our model results show that enhanced modeled sulfate burden and aerosol optical depth (AOD) persists for five years, while the volcanic halogens stay elevated for nearly 15 years. As a consequence the eruption leads to a collapse of the ozone layer with global mean column ozone values dropping to 50 DU (80 % decrease) leading to a 550 % increase in surface UV over the first five years with potential impacts on the biosphere. The volcanic eruption shows an asymmetric hemispheric response with enhanced aerosol, ozone, UV, and climate signals over the Northern Hemisphere (NH). Surface climate is impacted globally due to peak AOD of > 6 leading to a maximum surface cooling of >6 K, precipitation and terrestrial net primary production (NPP) decreases of >25 %, and sea ice area increases of 40 % in the first three years. Locally, a wetting (>100 %) and strong increase of NPP (>700 %) over Northern Africa is simulated in the first five years related to a southwards shift of the Inter-Tropical Convergence Zone to the southern tropics. The ocean responds with El-Niño conditions in the first two years which are masked by the strong volcanic induced surface cooling. Recovery to pre-eruption ozone levels and climate takes 15 and 30 years respectively. The long lasting surface cooling is sustained by sea ice/ocean changes in the Arctic showing an immediate sea ice area increase followed by a decrease of poleward ocean heat transport at 60° N lasting up to 20 years.

In contrast, when simulating Los Chocoyos conventionally, including sulfur and neglecting halogens, we simulate larger sulfate burden and AOD, more pronounced surface climate changes and an increase of column ozone. Comparing our aerosol chemistry ESM results to other super-eruption simulations with aerosol climate models we find a higher surface climate impact per injected sulfur amount than previous studies for our different sets of model experiments, since CESM2(WACCM6) creates smaller aerosols with a longer lifetime partly due to the interactive aerosol chemistry. As the

model uncertainties for the climate response to super eruptions are very large observational evidence from paleo archives and a coordinated model intercomparison would help to improve our understanding of the climate and environment response.

1 Introduction

The Los Chocoyos (LCY) super-eruption (Magnitude M_v=8 (Kutterolf et al., 2016), dated to 80.8±6.7 kyrs before present (Cisneros et al. to be submitted), was already 30 years ago assumed to be one of the largest volcanic eruptions of the past 100,000 years (Drexler et al., 1980). Originating from present-day Guatemala, the eruption formed the current stage of the large Atitlán caldera. Los Chocoyos released more than ~1100 km^3 of tephra and the eruption is used as a widespread key stratigraphic marker during that time (Cisneros et al., to be submitted; Kutterolf et al., 2016). The ash layers can be found in marine deposits from offshore Ecuador to Florida over an area of more than 10^7 km2 (Kutterolf et al., 2016). Hardly anything is known about the climate impacts of this eruption from proxy records, but LCY emitted large amounts of climate and environmentally relevant gases including sulfur, chlorine and bromine compounds (Krüger et al., 2015; Kutterolf et al., 2015, 2016; Metzner et al., 2014).

The sulfur gases emitted by volcanoes have a strong direct climate impact through the formation of sulfuric acid aerosols which blocks incoming sunlight and cools the surface (Robock, 2000). Halogen compounds, like chlorine and bromine, contributes to catalytic ozone depletion in the stratosphere (Brasseur and Solomon, 2005; Solomon, 1999). There is well-documented petrological evidence that large to extremely large explosive volcanic eruptions emitted environmentally significant amounts of chlorine and bromine (Cadoux et al., 2015, 2018; Krüger et al., 2015; Kutterolf et al., 2013, 2015; Vidal et al., 2016). Furthermore, recent atmospheric observations revealed that even relatively small volcanic eruptions can inject significant amounts of halogen compounds in the stratosphere (for review and overview discussions see (von Glasow et al., 2009; Krüger et al., 2015; WMO, 2018). Next, a sulfur and halogen rich eruption is expected to cool the Earths' surface and potentially damage the stratospheric ozone layer, with further impacts on the surface environment through the change in the atmosphere's transparency to harmful ultraviolet (UV), particularly shortwave UV-B, radiation (i.e. Brenna et al., 2019).

A simplified model approach of LCY was presented in Metzner et al. (2014). In this study, the General Circulation Model (GCM) MAECHAM5-HAM coupled with a modal aerosol microphysics scheme was used together with the Earth System Model of Intermediate Complexity (EMIC) CLIMBER-2 to study the climate impact of LCY based on the former published mass estimate of 687 Mt SO_2 (M_v=7.9) (Metzner et al., 2014). They simulated a peak cooling of 3.1°C from their LCY eruption scenario. Toohey et al. (2011, 2013) investigated atmospheric physical processes of LCY, using 700 Mt SO_2 injections with the model MAECHAM5-HAM, revealing the important effects of different seasons of that eruption on the aerosol evolution, transport, and deposition of sulfate to the ice cores and compared them to weaker eruptions strengths.

Even though there is little literature about LCY, the climate impact of super-eruptions has been discussed in the scientific

65 literature since at least the early 1990s. Early studies argued that the eruption of Toba (73 kyrs) could have initiated a glacial

period (Rampino and Self, 1992, 1993; Zielinski et al., 1996). In addition, there is evidence that human populations went

through a genetic bottleneck (i.e., most of the population died) at approximately the same time as the eruption of Toba

(Ambrose, 1998; Haslam and Petraglia, 2010; Williams et al., 2009), which has since been ruled out as unlikely (Timmreck

et al., 2010, 2012).

70 A thorough investigation of the climate impacts of very large volcanic eruptions (M_v: 7-8) requires the use of comprehensive

coupled climate models or, ideally, Earth System Models (ESMs). There are several published simulation studies of such

eruptions, mostly focusing on the Toba eruption, and the climate impact of it's sulfur injection. Bekki et al. (1996) used a

two-dimensional chemistry transport model with internally generated atmospheric circulation to study the Toba eruption

impact on the atmosphere. Their simulations indicate that Toba could have caused a long-lasting atmospheric response due

75 to the interactions between chemistry and aerosol microphysics.

Later, Jones et al. (2005) used a coupled atmosphere-ocean general circulation model (AOGCM) to study the Toba eruption

impact on climate. In this study they forced the model by linearly scaling the observed aerosol optical depth (AOD) from the

1991 eruption of Mt. Pinatubo by a factor of 100, resulting in peak cooling of ~11 K in the 2nd post-eruption year, followed

by an initial recovery taking a decade. Surface cooling larger than 1 K persisted for more than 20 years. The volcanic aerosol

80 forcing only lasted 5 years, so the response needed to be maintained by feedbacks in other components of the Earth System

through, i.e., sea-ice/ocean feedbacks sustaining the short atmospheric forcing to longer (decadal to centennial) time scales

(Miller et al., 2012; Stenchikov et al., 2009; Zhong et al., 2011).

In a similar study, Robock et al. (2009) used three different AOGCMs to study the Toba eruption effect on climate and

ozone. In their study, both the linear scaling AOD approach and directly injecting sulfur into a model with an interactive

85 bulk aerosol module were utilized. The resulting magnitude and length of the cooling was similar to what was published in

Jones et al. (2005) across the different model versions and forcing methods. The scenarios representing a 100 times Pinatubo

forcing resulted in ~12 K peak cooling with multi-decadal recovery times. In a 300 times Pinatubo scenario simulation

including atmospheric chemistry effects, Robock et al. (2009) found slightly stronger (~1 K) and much more long-lasting

surface cooling (length of >10 K cooling extended by ~5 years) compared to the similar forcing scenario without chemistry,

90 due to depletion of atmospheric hydroxyl (OH) limiting the speed of aerosol formation, leading to a longer-lasting forcing. In

addition, they simulated an increase in global column ozone, attributed to the reduction of reactive hydrogen oxides in the

atmosphere.

Another model study of Toba, presented in Timmreck et al. (2010, 2012), simulated a smaller climate impact with peak

cooling of 3.5 K lasting up to 10 years from injected sulfur compared to the analogous simulations in Robock et al. (2009). A

95 key difference between Timmreck et al. (2010) and previous AOGCM simulations of Toba is the inclusion of online aerosol

microphysics in a modal aerosol scheme and the OH limitation mechanism, leading to larger aerosol sizes, lower peak AOD

(~4) values and thus lower climate impacts in Timmreck et al. (2010). The inclusion of interactive OH chemistry in the

formation of aerosol is important because the availability of OH controls the speed of SO_2 oxidation into sulfate (Bekki, 1995).

100 Concentrating on the atmospheric processes, English et al. (2013) used a sectional aerosol microphysical model coupled to a chemistry climate model with prescribed sea surface temperatures (SSTs) to study the aerosols and atmospheric impacts of the Toba eruption. In their model setup, neglecting aerosol radiative heating, they simulate even lower peak AOD values (~2.6) due to the fact that their sectional aerosol module creates larger aerosols compared to Timmreck et al. (2010).

In the climate modeling literature on the Toba super eruption there is a progression from larger climate (and environmental)
105 impacts to smaller as models complexity develop over time. One key seems to be that climate effects are self-limiting for larger eruptions due to an increase of aerosol growth which reduces peak AOD (English et al., 2013; Pinto et al., 1989; Timmreck et al., 2010). In addition, the role of atmospheric chemistry and OH limitation on sulfuric acid aerosols is continuously under discussion in the literature (Bekki, 1995; Mills et al., 2017; Niemeier et al., 2019; Robock et al., 2009; Timmreck et al., 2003).

110 Investigating the effects of the Toba eruption on the earth system such as hydrology and terrestrial net primary production reveals a substantial reduction of precipitation globally leading to reduction of tree cover, increase of grass cover and decreased NPP, but with large regional and inter-model variability (Robock et al., 2009; Timmreck et al., 2010, 2012). While tropical deciduous trees and broadleaf evergreen trees virtually disappear in the simulations of Robock et al. (2009), Timmreck et al. (2011) find much more muted impacts on tree cover, particularly in the Tropics. Timmreck et al. (2011)
115 even simulate an increase of NPP in the tropical rain forest regions of South America and Africa.

We are not aware of studies of super-size eruption effects on sea ice/ocean and the El Niño Southern Oscillation (ENSO), whereas the effects of large to very large volcanic eruptions have been widely discussed in the literature. Recent studies proposed a sea ice/ocean mechanism which prolong the volcanic induced short, abrupt surface cooling and sea ice increase to longer time scales (decadal) with the ocean sustaining the signal by buffering and transporting the cooling poleward
120 (Miller et al., 2012; Zhong et al., 2011). With regard to volcanoes and ENSO, there is an ongoing debate (Stevenson et al., 2017) that tropical volcanic eruptions can either lead to La Niña-like response in the same year (Anchukaitis et al., 2010; Li et al., 2013) or the following (five) years (Zanchettin et al., 2012) or to El Niño-like response up to the two following years (e.g., (Adams et al., 2003; Handler, 1984; Khodri et al., 2017; Ohba et al., 2013; Stevenson et al., 2016)). Discussions include the significance and mechanism of the results as well as the eruption characteristics, latitude, season, and strength.

125 Simulations of halogen (and sulfur) rich eruptions show that these can have serious, long-lasting impacts on the ozone layer, with implications for the surface environment through the increase of surface ultraviolet radiation. In a study of the ~1 Myr period of extremely large effusive eruption of the Siberian Traps (~250 million years ago) (Black et al., 2014), a near-total elimination of the ozone layer was found, as well as massive increases in surface ultraviolet radiation (~10 years recovery time after cessation of emissions), Black et al. (2014) hypothesized that this could be a contributing mechanism to the
130 Permian-Triassic mass extinction at that time. In a 2D chemical transport model (CTM) study of the late Bronze Ager eruption of Santorini (magnitude 7), Cadoux et al. (2015) simulated decadal ozone depletion, mainly in the northern

hemisphere, with peak depletion of 20-90 % depending on the degassing budget. In another study using a 2D CTM (Klobas et al., 2017), (hypothetical) volcanic halogens were included with the sulfur injection of Mt. Pinatubo, showing ozone depletion of 20 % lasting a few years under different future emission scenarios. Using CESM1(WACCM) a comprehensive

135 coupled chemistry climate model (CCM), with prescribed volcanic aerosols and SSTs, Brenna et al. (2019) simulated an average Central American Volcanic Arc (CAVA) eruption with magnitude 6.4. They found ozone depletion up to 20 % globally lasting up to 10 years, which were most pronounced over the Northern Hemisphere (NH) and dropped below present day ozone hole conditions over Antarctica and the tropics. Consequently, surface UV radiation increased by >80 % over the 2 years with potential impacts on human health, agriculture and marine life.

140 Despite the Siberian Trap volcanism studies (Beerling et al., 2007; Black et al., 2014), we are not aware of super eruption studies taking the combined effect of sulfur and halogen injections in a fully coupled aerosol chemistry climate/ earth system model into account.

In this study we use the recently released CESM2 coupled with WACCM6 as the atmospheric component, which allows us to investigate newly the coupling and the feedbacks between volcanic aerosols, chemistry, radiation, climate and the earth

145 system after a sulfur and halogen rich super volcanic eruption. In this paper, we present the climate and environmental impacts of the sulfur- and halogen-rich super eruption Los Chocoyos (Guatemala, 80.6 kyrs ago; Cisneros et al. to be submitted). In a forthcoming paper, we will investigate the impacts on the atmospheric circulation.

2 Methods

2.1 Los Chocoyos erupted volatile estimates

150 Using the recently published total erupted mass estimate for the LCY eruption (Kutterolf et al., 2016) and the previously published petrologic estimates of volatile concentrations for sulfur, chlorine and bromine (Kutterolf et al., 2013, 2015; Metzner et al., 2014) we calculate a new mass of erupted volatiles for LCY as a starting point for defining the stratospheric injections in our model simulations. The erupted volatile masses as calculated using these estimates are 523±94 Mt sulfur, 1200±156 Mt chlorine and 2±0.46 Mt bromine.

155 2.2 CESM2(WACCM)

In this study we use the Community Earth System Model Version 2 (CESM2) (Danabasoglu et al., to be submitted) coupled with the Whole Atmosphere Community Climate Model Version 6 (WACCM6) (Gettelman et al., submitted to JGR) as the atmospheric component. CESM2(WACCM6) is a comprehensive numerical model spanning the whole atmosphere from the surface to the lower thermosphere with model top at ~140 km altitude. The chemistry module includes the SOx, Ox, NOx,

160 HOx, ClOx and BrOx chemical families, implementing 98 compounds and ~300 reactions. It covers gas-phase, photolytic and heterogeneous reactions on three types of aerosols including polar stratospheric clouds which form interactively in the

model. Stratospheric sulfuric acid aerosols are formed interactively from sulfur compounds and modeled by the modal aerosol model MAM4 (Liu et al., 2016), which has been adapted and extended for the stratosphere (Mills et al., 2016). CESM2(WACCM6), as a coupled CCM, allows us to explore the coupling between radiation, temperature, circulation,

165 chemistry and composition in the atmosphere. The horizontal resolution is 0.95° longitude by 1.25° latitude with 70 hybrid sigma pressure layers from the surface to 5.5e-6 hPa. The quasi-biennial oscillation (QBO) is internally generated (Gettelman et al., submitted to JGR).

The ocean model of CESM2(WACCM6) is POP2 running at ~1×1 degrees horizontal resolution with 60 layers in the vertical. CICE5 is the sea ice model for CESM2(WACCM6) (Bailey et al., CESM CICE5 Users Guide, NCAR

170 documentation, PP. 47, June 2018) which is running at the identical grid as POP2. The land surface model in CESM2(WACCM6) is the community land model Version 5 (Fisher et al., 2019).

2.3 Model experiments

To model the impact of the LCY eruption on the atmosphere we use the petrological estimated erupted sulfur and halogen masses as input. We inject all of the erupted sulfur mass as SO_2 and 10 % of the erupted halogen mass, as HCl and HBr, into

175 the stratosphere, which we consider a conservative estimate given the range of available observational and plume model evidence (see the detailed discussion in Krüger et al. 2015 and Brenna et al. 2019). The volcanic volatiles are injected into the model grid boxes at 14.6°N and between 80° and 97.5°W, at 24 km altitude. The eruption date is set to 1. January, as the eruption season is not known, and needed to be spread over the first 6 days in the model to allow the massive volatile mass to accumulate over time and neighboring longitudinal grids.

180 We run an ensemble of six simulations for the combined sulfur and halogen forcings (**LCY_full**) starting from different ENSO (positive, negative, neutral) and QBO (easterly, westerly) states of the control run (**Ctr**). In addition, we perform two simulations (QBO easterly and westerly, ENSO neutral, branching from the same **Ctr** years as for **LCY_full**) with only the sulfur forcing (**LCY_sulf**) to explore the difference in response between the forcing scenarios. All ensemble members last 35 years. The control simulation is 70 years with constant 1850 forcings. In all simulations, background stratospheric

185 concentrations of chlorine and bromine are 0.45 ppbv and 10.2 pptv at the 10 hPa level respectively, consistent with preindustrial estimates (WMO, 2014). In addition to these main experiments, we have performed two sensitivity simulations. One with sulfur injection reduced by a factor of 100 (**LCY_1%sulf**) and one with full sulfur injection and 1 % halogen injection efficiency instead of 10 % (**LCY_1%halog**). The experiments are summarized in Table 1.

2.4 Surface UV calculations

190 We calculate the UV radiation at the surface using the Tropospheric Ultraviolet and Visible (TUV) radiation transport model (Madronich and Flocke, 1997) using similar methods as in Brenna et al. (2019). In our setup, TUV solves the radiative transfer equations given the parameters: Date of the year, position, time of day, column ozone values and total AOD at 550 nm taking aerosol scattering into account. We run the TUV model offline for each point in latitude and longitude and using

hourly temporal resolution to get a representation of the variations in UV throughout the year. As input to the TUV model
195   we give averages of column ozone and AOD over the first five years after the eruption for LCY_full and LCY_sulf and for
the control run to generate UV fields for the eruption scenarios and for the control run climatology.

2.5 Oceanic Niño Index (ONI)

To select initial conditions for the set-up of the ensembles and to quantify the impact of the volcanic eruptions on the ENSO
we calculate the Oceanic Niño Index (ONI) using the model output. An ENSO positive or negative phase is defined as
200   ONI>0.5 or ONI<-0.5, respectively, for more than 5 consecutive months.

3 Results and discussion

3.1 Atmospheric burdens of volcanic gases and aerosols

Using our modeling approach results in the atmospheric burdens of volcanic gases and aerosol distinguishing between
burden anomalies and the same burdens, normalized by the respective maximum values as summarized in Figure 1.
205   The normalized total sulfur burden after the simulated eruptions has an e-folding time (reduction by 1/e) of a little more than
two years (Figure 1b). There is first a plateau for ~1 year before decay starts. The following e-folding times ($1/e^2$ and $1/e^3$)
are shorter, a bit less than 1 year. After ~5 years most of the sulfur has been removed from the atmosphere. The total sulfur
burden life times are remarkably similar for all four injection scenarios, even when the injection amounts differ by a factor of
100. In contrast, the halogens have a longer e-folding time of approximately 3 years, but the following e-folding times for
210   $1/e^2$ and $1/e^3$ are ~1 year, similar to what we simulate for total sulfur.

The conversion of injected SO_2 into sulfuric acid aerosol is significantly slowed down in the LCY_sulf, LCY_full and
LCY_1%halog scenarios compared to the LCY_1%sulf, where we only injected 1 % of the sulfur (Figure 1 d). The e-folding
time of the SO_2 burden increases from ~3 months to ~6 months when the injected SO_2 mass is increased by a factor of 100.
There is an additional increase in lifetime to ~1 year when halogens are injected in addition to SO_2. This increase in SO_2
215   lifetime is caused by the limited oxidizing capacity of the atmosphere (see also Bekki et al. 1995). The main compound
responsible for oxidizing SO_2 to sulfuric acid is OH. When the SO_2 burden increases the availability of OH is limited and
oxidation slows down. When halogens are injected in addition, reactions involving halogens also consume OH (Fig. 1f)
further limiting the OH available for SO_2 oxidation, and thus further increasing the SO_2 lifetime (Fig. 1d).

The peak aerosol mass, when the sulfur burden is the same, is depending on the conversion time of SO_2 into aerosol. Thus,
220   the peak aerosol mass is lower in the LCY_full scenario compared to the LCY_sulf (Figure 1c). Even though the peak
burdens are different, the lifetime of the aerosol mass perturbation is very similar in the two cases (Figure 1d), indicating that
the removal mechanisms in these scenarios are very similar. The global mean weighted aerosol effective radius is small and
very similar in these two scenarios, while in the LCY_1%sulf the aerosols have much smaller effective radii (factor ~3.5

smaller) (Figure 1e), as expected when the injection is smaller (English et al., 2013; Pinto et al., 1989; Timmreck et al.,
225   2010). Even though the aerosols are smaller in the LCY_1%sulf simulation, the removal time scale for the aerosols is similar
to the two other scenarios, This indicates that gravitational settling, which is not important for sub-micrometer aerosols
(Seinfeld and Pandis, 2016), is playing a minor role as a removal mechanism for the aerosol mass, and removal processes
will tend to happen on the transport time-scale of the stratosphere.

Since the maximum aerosol mass in the LCY_sulf is ~25 % larger compared to the maximum mass in LCY_full, while the
230   aerosol sizes are approximately the same, we find that the peak AOD at 550 nm is much larger in the LCY_sulf scenario
(>8) compared to the LCY_full scenario (~6) (Figure 2a). This translates into a larger energy imbalance at the top of the
model in LCY_sulf (Figure 2b). The maximum radiative imbalance at the top of the model is approximately -50 W/m^2 in the
LCY_sulf and -40 W/m^2 in the LCY_full scenario. In both cases, an initial strong negative net imbalance is followed by a
small positive net imbalance after ~3.5 years, and throughout the climate recovery period.

235   3.2 Ozone and UV response

Global ozone collapses after the eruption in the LCY_full scenario, with whole column values decreasing by >80 % to a
global mean value of 50 DU (a measure of the thickness of the ozone layer) during years 2-3 after the eruption (Figure 3a).
Ozone levels lower than present-day Antarctic ozone hole conditions (<220 DU) persist for 8 years over the whole globe
(Figure 3a, S1). Depletion shows a bi-modal distribution in the stratosphere, with maximum depletion in the upper (~4 hPa)
240   and lower (~30 hPa) stratosphere (Figure S2). In the lower stratosphere, where most of the ozone mass is located, >70 % of
ozone is destroyed after 1 year, and this level of depletion persists for 7 years (not shown). Peak depletion in the lower
stratosphere is >95 %. Significant global mean ozone column reduction lasts for ~12 years. In the Antarctic, ozone hole
conditions continue re-occurring annually for 16 years (Figure S1b). Compared to LCY_full, the ozone response in
LCY_1%halog is smaller, but reveals a similar response. A substantial decrease to global mean column values of ~150 DU
245   and a recovery after about 10 years; a larger and longer lasting ozone response as was simulated for an average CAVA
eruption with magnitude 6 and 10 % halogen injection efficiency (Brenna et al. 2019).

In contrast, in the LCY_sulf scenario, the column ozone increases by more than 100 DU in the first year after the eruption
(Figure 3a). This is caused by the increase in heterogeneous chemistry taking place on the sulfate aerosols which reduces the
concentrations of ozone-destroying NO$_X$ (Tie and Brasseur, 1995) and was modelled for large and super-size volcanic sulfur
250   injections into a pre-industrial stratosphere with low chlorine background levels (Muthers et al., 2015; Robock et al., 2009).
The ozone increase decays in about 3 years and is only slightly elevated after that until post-eruption year 10 (Figure 3a).
The increase in ozone is concentrated in the mid to high latitudes and mostly in the NH (Figure S1c).

In Figure 4 we present global maps of total AOD (a,b), as well as anomalies and the climatologies for column ozone and
surface UV (g,h) averaged over the first five years (pentade) after the eruption for both the LCY_full and LCY_sulf
255   scenarios. The spatial pattern in AOD is similar between the LCY_full and LCY_sulf scenarios with larger AOD anomalies

in the extratropics compared to a band of low AOD in the Southern Hemisphere (SH) tropics, and the largest impacts in the NH (Figure 4 a, b). In LCY_full, AODs are smaller over Antarctica than at lower latitudes. This might be as transport to the Antarctic region is suppressed by the strengthening of the Westerlies winds surrounding the southern polar vortex (not shown here), which acts as a transport barrier for the volcanic aerosols (Toohey et al., 2013). In LCY_sulf the global mean

260   AOD is larger (c.f. Figure 2a), which holds for the local distribution over the globe as well (Figure 4a+b).

Figure 4g and h shows the calculated change in the amount of surface ultraviolet radiation (UV-B) weighted for DNA damage calculated using the radiation transport model TUV (see Methods). Taking into account both the change in AOD and the change in column ozone in the TUV calculations we find very large, but opposite signals in the two eruption scenarios. In the LCY_full scenario, the largest increases in surface UV are more than 1400 % in the Arctic and more than 1000 % in

265   the Antarctic. Changes are generally smaller towards the equator, but no part of the planet experiences less than a 200 % increase. Global average increase over the five-year period is 545 % (Figure 3b). By contrast, in the LCY_sulf scenario the UV-B decreases by more than 80 % in the mid-to-high latitudes of the NH and by >60 % over most of the rest of the planet (Figure 4g,h). The UV response in our calculations are impacted by the ozone levels and the AOD (Figure 4a-f), and in LCY_full the AOD and ozone effects are opposing each other with the ozone effects being strongest, while in LCY_sulf they

270   are both contributing to a decrease in surface UV.

3.3 Climate and environmental response

3.3.1 Global surface temperature decreases for 30 years

Time series of global mean surface temperatures are shown in Figure 3b. For both scenarios, global mean surface temperature decreases more than 6 K and is back to climatological background after approximately 30 years. The difference

275   between the LCY_full and LCY_sulf forcing scenarios is >1 K at peak cooling in year 2. If the aerosol response from the sulfur injection (which is the same in these two scenarios) was the same, we would expect the temperature response to be very similar, and perhaps LCY_full would be slightly cooler since ozone depletion in the stratosphere is a negative radiative forcing on the global climate system (Myhre et al., 2013). Instead, we interpret this difference in surface temperature response due to the large difference in peak AOD (Figure 2a).

280   In Figure 5 (a, b) we show pentadal average maps of surface temperature anomaly for both the LCY_full and LCY_sulf scenarios. Temperature anomaly patterns are relatively similar between the scenarios with surface cooling almost globally and largest anomalies in the NH and over the continents. The magnitudes are large (larger in LCY_sulf, c.f. Figure 3b), even in a five year mean, with most continental areas experiencing at least 4 K cooling, locally dropping <10 K over central Asia (Figure 5a,b).

3.3.2 Sea-ice/ocean changes for 20 years

The long lasting global cooling response cannot be explained by the direct radiative forcing from the volcanic aerosols, since the aerosols have mostly disappeared after 5 years. In Figure 3c we show the 12 month running mean change in global mean sea ice area. Sea ice immediately response to the eruption induced surface cooling with a peak increase of sea ice area globally up to 40 % in LCY_full and up to 50 % in LCY_sulf. Global sea ice area in the model experiments is not back to climatological values before at least 20 years after the eruption. When inspecting NH sea ice and ocean changes more in detail (Figure S4) we find that Arctic sea ice area is increased immediately after the eruption and for more than 20 years with a maximum of 7 million km^2 (not shown), a 104 % increase in post-eruption year 2. This change is accompanied by a reduction of ocean heat content (not shown) and a decrease of poleward ocean heat transport at 60° N after the eruption, lasting from post-eruption year 3 up to 20 with a maximum decrease up to 0.1 PW (20 %) in post-eruption year 5 (Figure S4). Thus, abrupt surface cooling and decrease of upper ocean heat content in the NH leads to an immediate increase of Arctic sea ice area in the first years. The reduced poleward ocean heat transport at northern mid-latitudes for up to 20 years sustains the sea ice and climate surface cooling signal for more than 20 years in the NH and also globally. Antarctic sea ice area reveals a slightly later and shorter lasting increase from post-eruption years 1 to 5. The poleward ocean heat transport at 60°S is much more variable than in the NH and does not show significant changes over longer time periods in our simulations. This may be due to the later supply of AOD to the southern hemisphere (SH) (Figure S1), thus later radiative forcing, as well as smaller AOD and hence weaker surface climate response in the SH compared to the NH (Figures 4, and 5). For a tropical January eruption, AOD is first distributed in the tropical belt in the first few weeks before being transported poleward to the NH winter/spring season and then to the SH in the following months (Figure S1; see also Toohey et al., 2011), reflecting the pathways and seasonality of the Brewer Dobson circulation (Plumb, 2002). Atmospheric circulation changes are expected to be significant for the LCY eruption as was shown by Toohey et al. (2011, 2013) and will be further investigated in a follow up paper.

3.3.3 Large impacts on precipitation and vegetation

A strong cooling of the atmosphere, like from an explosive volcanic eruption, leads to decreased precipitation (Robock and Liu, 1994). In our simulations, global mean precipitation (Figure 3d) decreases ~25 % (~0.8 mm/day) in the LCY_full scenario and more than ~30 % (1 mm/day) in the LCY_sulf scenario. The LCY_sulf simulation is outside the two standard deviation range of the LCY_full ensemble. Return to background climatological precipitation takes more than 10 years in both scenarios. The minimum precipitation is found between 2 and 3 years after the eruption, closely following the drop in the temperature signal.

Pentadal precipitation patterns are similar in both scenarios (Figure 5 c-f), with drying over approximately two thirds of the planet, a distinct southward shift of the Inter-Tropical Convergence Zone (ITCZ) in the Pacific and Atlantic to the SH tropics and wetting on the subtropical east sides of the oceanic basins. In addition, there is a pronounced wetting signal (>100 %)

throughout the tropical East Atlantic, Northern Africa, Middle East, and the Arabian Peninsula. These are relatively dry regions, so a moderate absolute increase in precipitation (<1 mm/day) corresponds to more than a doubling of rainfall over large parts of this region. Comparing LCY_full and LCY_sulf, the impacts are generally stronger for the latter scenario both

320   where we find drying and wetting.

The strong AOD increase, global surface cooling and decrease in precipitation together results in a decrease in land plant productivity (Net Primary Production (NPP) of >30 % during the first three years after the eruption, followed by suppressed production during the next ~15 years (Figure 3d). NPP is especially reduced over the NH land with peak decrease >75 % over high latitudes and a gradual weakening of this signal towards lower latitudes (Figures 5g,h and S3). However, over

325   Northern Africa and surrounding areas, where precipitation increases significantly due to the southward shift of the ITCZ, we find a corresponding enhancement in land plant productivity as shown by a strong increase in NPP in this region. This is by far the strongest signal we detect in NPP with more than 400 % gain in some areas.

3.4 El Niño conditions

330   The ENSO response of the simulations is shown in Figure 6. Even though the initial conditions of the experimental set-up span different ENSO states, there is a rapid convergence to a robust response in the two eruption scenarios, ONI values drop below -5 during the first 5 years after the eruption. First, the LCY_full ensemble spread is suppressed for 3 years after the eruption, before beginning to diverge again. The ONI values drop far below the range of natural variability, but there are two local maxima during post-eruption years 0 and 1, with an amplitude similar to a strong El Niño in the control simulation.

335   Thus, we compare the ensemble mean of these temporal peaks to the ensemble mean average temperature over post-eruption years 0-5 and 1-4, respectively. The resulting spatial patterns are shown in Figure 6b and c. Compared to the dominant volcanic surface cooling pattern, these maxima represent El Niño conditions, indicating that the super volcanic eruption is triggering an El Niño response in the first two years after the January eruption, which is masked by the strong surface cooling caused by the eruption.

340   **4. Comparison with other studies**

Our simulations show very large climate impacts from the LCY sulfur- and halogen-rich super-eruption, and a break from the tendency towards simulating smaller climate impacts from the Toba eruption, that we noted in the Introduction. In Figure 7 we show scatter plots comparing our simulations of LCY to other simulations of super volcanic eruptions using sulfur only injections (English et al., 2013; Jones et al., 2005; Metzner et al., 2014; Robock et al., 2009; Timmreck et al., 2010).

345   Compared to other model studies with interactive aerosols of volcanic eruptions of magnitude $M_v > 7$, our simulations show very large maximum AODs and thus maximum surface climate impacts for a given sulfur injection (Figure 7 a, b). The largest climate cooling for a super eruption is achieved when using linearly scaled AOD values based on Pinatubo (Jones et

al., 2005; Robock et al., 2009), but this approach is simplified, since there are several feedbacks (i.e., self-limiting, scattering, and removal of aerosols) that makes the relationship between sulfur injection, aerosols, radiative forcing, and

350 climate highly non-linear i.e. (Bekki, 1995; Metzner et al., 2014; Pinto et al., 1989).

Limiting our comparison to model studies that use sulfur injection to generate self-consistent AOD estimates, we see that our model experiments show larger radiative impacts and larger surface cooling per injected sulfur mass to the stratosphere than those studies (English et al., 2013; Metzner et al., 2014; Timmreck et al., 2010). The differences could be caused by different aerosol microphysics (bulk vs. modal vs sectional modules), radiation, advection and depositions schemes (see

355 discussions by English et al 2013; also Marshall et al. (2018) for a discussion), as well as atmospheric chemistry (OH, ozone, H_2O) and climate/ESM model differences (coupling, resolution, clouds). Our comparison (Figure 7) is limited by the fact that the simulations were not part of a coordinated model intercomparison yet, thus the model experiments are all different related to eruption strength, date, location, and injection altitude. Volcanic aerosol climate model intercomparisons are in progress now (see (Timmreck et al., 2018; Zanchettin et al., 2016)) and should include extremely large to super-size

360 eruptions, where the model spread is even larger (Figure 7) but observational evidence is lacking.

Even though the halogen injection efficiency for a super eruption like LCY is highly uncertain, we expect that the effects of injected halogens would be qualitatively similar independent of the magnitude of the injection as our model results for 10 % and 1 % halogen injections revealed. Injecting additional volcanic halogens into the stratosphere leads to ozone depletion (this study; (Brenna et al., 2019) and the interaction with the OH availability impacts the aerosol formation leading to

365 smaller maximum AOD and hence weaker surface cooling. Including the volcanic release of halogens as well as sulfur should be a part of future model intercomparisons focusing on volcanic impacts on climate and ozone.

Overall, the model uncertainties for super eruptions is dramatically reduced when comparing the peak climate response to a given maximum AOD (Figure 7), which shows a clear relationship, slightly non-linear, with decreasing surface temperature with increasing AOD.

370 When atmospheric temperatures drop after a volcanic eruption, changes in energy balance of the climate system leads to decreased global mean precipitation (Iles et al., 2013; Robock and Liu, 1994). The global mean precipitation response to the super volcanic eruptions follows a nearly linear relation with temperature (Figure 7d), larger cooling leads to larger negative precipitation anomalies through a weakening of the global hydrological cycle since lower temperatures leads to lower relative humidity in the troposphere. Our modeled southward shift of the ITCZ towards the southern tropics is accompanied

375 by increased precipitation across North Africa and the Middle East, which is partly simulated also in Robock et al. (2009) and Timmreck et al. (2010, 2012), but the area experiencing wetting is larger in our simulations. The wetting of North Africa and the Middle East in our simulations leads to a strong increase in NPP in this area and thus likely to a greening of the Sahara. Timmreck et al. (2012), with only half the volcanic forcing that we simulate, shows NPP maps (vegetation impacts are simulated using an off-line vegetation model), and here there is very little change over the first three post-eruption years

380 throughout this region. While we cannot compare our NPP field directly to the changes in vegetation types presented in Robock et al. (2009), we note that they simulate an increase in grass cover throughout North Africa and parts of the Middle

East where there is very low vegetation cover in their control run, which would imply an increase in NPP in this region as well.

We simulate El Niño conditions to our LCY super eruption during the first two post-eruption years, but superposed on a strong surface cooling signal. El Niño conditions may be favored up two years as discussed in more detailed by Emile-Geay et al. (2008) due to the uniform solar dimming leading to a thermostat mechanism (Clement et al., 1996) initiating air-sea interaction in the equatorial Pacific. Our simulations of the sulfur- and halogen-rich LCY super eruption in the Northern tropics (15° N) during January adds another puzzle piece to the ongoing discussion of volcanic eruption impacts on ENSO (see Introduction). A coordinated model intercomparison study would help to shed more light into the different model response and mechanism.

Atmospheric circulation changes (i.e., stratospheric polar vortices, Annular Modes) are expected to be significant as was shown by Toohey et al. (2011, 2013) and will be further investigated in a follow up paper.

Using a fully coupled ESM with interactive aerosols and atmospheric chemistry is currently the best possible way to simulate the impacts of super-volcanoes on the Earth system. Our model setup takes into account the interactive coupling between most of the components of the Earth system, including ocean, sea-ice, bio-geochemistry, land surface and vegetation interactions. In addition, the inclusion of interactive aerosols and atmospheric chemistry is crucial to correctly simulate the feedbacks between the chemical composition of the atmosphere, aerosols and radiation. That said, there is still considerable uncertainty in the impacts of volcanic sulfur injections, particularly in the conversion of SO_2 into sulfate aerosol, aerosol size and the lifetime of the radiative perturbation. The uncertainty in the Earth system's reaction to a given volcanic aerosol radiative forcing seems to be smaller (c.f. Figure 7c). Based on our set of model experiments and sensitivity studies next to existing model studies on the volcanic impact on ozone (Black et al., 2014; Brenna et al., 2019; Klobas et al., 2017; Muthers et al., 2015; Robock et al., 2009), we evaluate the ozone response for volcanic sulfur and halogen injections into the stratosphere currently to be more robust than for the climate response to a given sulfur injection.

Finally, LCY may be the super eruption of the last 100 kyrs as a slightly higher sulfur mass loading was just released (Cisneros et al. to be submitted) and Toba is estimated to be less sulfur rich than previously assumed (Chesner and Luhr, 2010). To compare these two super eruptions and petrological estimates other archives such as ice core records would be needed. However, no tephra has been identified in Greenland and Antarctica ice cores for both eruptions up to now (Abbott et al., 2012; Svensson et al., 2013). This model study together with the new dating of the LCY eruption to 80.8±6.7 kyrs and a higher (Cisneros et al., to be submitted) will hopefully stimulate upcoming studies finding corresponding paleo proxies in ice cores, climate, and archaeological archives.

5. Summary and conclusions

Our comprehensive aerosol chemistry Earth System Model (ESM) study shows that a sulfur- and halogen-rich tropical super-eruption like Los Chocoyos (LCY) has massive impacts on global climate and the environment lasting at least 20-30 years.

415 In the model, enhanced volcanic sulfate burdens and aerosol optical depth (AOD) persists for five years, while the halogens stay elevated for ~14 years. Under pre-industrial conditions, the eruption leads to a global collapse of the ozone layer (80 % decrease) with global mean values of 50 DU and increasing surface UV-B by 550 % globally over the first 5 years after the eruption. (In high latitudes the increase is >1000 %). The ozone layer takes 15 years to recover. The simulated volcanic eruption, at 15° N in January, shows an asymmetric hemispheric response with enhanced AOD, ozone, UV, and climate

420 signals over the Northern Hemisphere (NH).

The eruption cools the global climate lasting more than 30 years with the peak AOD of >6 leading to surface cooling >6 K and precipitation and terrestrial net primary production (NPP) decreases up to 30 % in the first two years. Locally, a wetting (>100 %) and strong increase of NPP (>400 %) over Northern Africa is simulated in the first five years related to a southwards shift of the Inter-Tropical Convergence Zone to the southern tropics. Global sea ice area almost doubles, and the

425 long lasting surface cooling is sustained by sea ice/ocean changes mainly in the Arctic showing an immediate sea ice area increase followed by a decrease of poleward ocean heat transport at 60° N from year 3, both changes lasting up to 20 years. The ocean responds with El-Niño conditions in the first two years which are masked by the strong volcanic induced surface cooling.

The long lasting surface cooling is sustained by sea ice/ocean changes showing an immediate sea ice area increase followed

430 by a decrease of poleward ocean heat transport at 60° latitude from year 3, both changes lasting up to 20 years.

In contrast, simulations of LCY including sulfur, but neglecting halogens, reveal larger sulfate burden and maximum AOD (~8), hence a larger radiative forcing with more pronounced surface climate cooling (>7 K) and reduced precipitation (25 %) globally, even though spatial patterns of changes are similar to the simulations including volcanic sulfur and halogens. The environmental impacts reveal the opposite signal with a short-lived increase of column ozone of 100 DU (>30 %) and

435 decrease of UV (>60 %) lasting up to 3 years.

LCY is one of the largest volcanic eruptions over the past 100 kyrs and we predict large impacts on the biosphere and thus any human populations at that time. Finding paleo proxies showing the impact of LCY on climate and the environment should be possible, given the large long lasting impact from our ESM simulations, but will require high (decadal) temporal-resolution archives using the eruption as a time marker.

6. Code and data availability

All simulation data will be archived in the NIRD Research Data Archive on acceptance of the manuscript. Post processing and visualization of data was performed with Python and the code and post processed data files are available on request from the corresponding author.

7. Supplement

The supplement related to this article is available online at:

8. Author contributions

HB performed the simulations, data analysis and produced the figures. HB, KK and SK interpreted the results. MM provided the CESM2(WACCM) model and supported HB in performing simulations. HB wrote the manuscript with contributions from all co-authors.

9. Competing interests

The authors declare that they have no conflict of interest.

10. Acknowledgements

The authors want to thank the CESM model team at NCAR for providing the CESM2(WACCM6) model code and for their technical model support. The simulations for this study were performed on resources provided by UNINETT Sigma2 - the National Infrastructure for High Performance Computing and Data Storage in Norway. The publication of this article is funded by the EGU through the 2018 Outstanding Student Poster and PICO Award for HB.

References

Abbott, P. M., Davies, S. M., Steffensen, J. P., Pearce, N. J. G., Bigler, M., Johnsen, S. J., Seierstad, I. K., Svensson, A. and Wastegård, S.: A detailed framework of Marine Isotope Stages 4 and 5 volcanic events recorded in two Greenland ice-cores, Quat. Sci. Rev., 36, 59–77, doi:10.1016/j.quascirev.2011.05.001, 2012.

Adams, J. B., Mann, M. E. and Ammann, C. M.: Proxy evidence for an El Niño-like response to volcanic forcing, Nature, 426(6964), 274–278, doi:10.1038/nature02101, 2003.

Ambrose, S. H.: Late Pleistocene human population bottlenecks, volcanic winter, and differentiation of modern humans, J. Hum. Evol., 34(6), 623–651, doi:10.1006/jhev.1998.0219, 1998.

465   Anchukaitis, K. J., Buckley, B. M., Cook, E. R., Cook, B. I., D'Arrigo, R. D. and Ammann, C. M.: Influence of volcanic eruptions on the climate of the Asian monsoon region, Geophys. Res. Lett., 37(22), doi:10.1029/2010GL044843, 2010.

Beerling, D. J., Harfoot, M., Lomax, B. and Pyle, J. a: The stability of the stratospheric ozone layer during the end-Permian eruption of the Siberian Traps., Philos. Trans. A. Math. Phys. Eng. Sci., 365(1856), 1843–66, doi:10.1098/rsta.2007.2046, 2007.

470   Bekki, S.: Oxidation of volcanic SO2: A sink for stratospheric OH and H2O, Geophys. Res. Lett., 22(8), 913–916, doi:10.1029/95GL00534, 1995.

Black, B. A., Lamarque, J. F., Shields, C. A., Elkins-Tanton, L. T. and Kiehl, J. T.: Acid rain and ozone depletion from pulsed siberian traps magmatism, Geology, 42(1), 67–70, doi:10.1130/G34875.1, 2014.

Brasseur, G. P. and Solomon, S.: Aeronomy of the middle atmosphere: Chemistry and physics of the stratosphere and
475   mesosphere, Planet. Space Sci., 644, doi:10.1016/0032-0633(85)90091-1, 2005.

Brenna, H., Kutterolf, S. and Krüger, K.: Global ozone depletion and increase of UV radiation caused by pre-industrial tropical volcanic eruptions, Sci. Rep., 9(1), 1–14, doi:10.1038/s41598-019-45630-0, 2019.

Cadoux, A., Scaillet, B., Bekki, S., Oppenheimer, C. and Druitt, T. H.: Stratospheric Ozone destruction by the Bronze-Age Minoan eruption (Santorini Volcano, Greece), Sci. Rep., 5(April), 12243, doi:10.1038/srep12243, 2015.

480   Cadoux, A., Iacono-Marziano, G., Scaillet, B., Aiuppa, A., Mather, T. A., Pyle, D. M., Deloule, E., Gennaro, E. and Paonita, A.: The role of melt composition on aqueous fluid vs. silicate melt partitioning of bromine in magmas, Earth Planet. Sci. Lett., 498, 450–463, doi:10.1016/j.epsl.2018.06.038, 2018.

Chesner, C. A. and Luhr, J. F.: A melt inclusion study of the Toba Tuffs, Sumatra, Indonesia, J. Volcanol. Geotherm. Res., 197(1–4), 259–278, doi:10.1016/j.jvolgeores.2010.06.001, 2010.

485   Cisneros de León, A., Schindlbeck-Belo, J. C., Kutterolf, S., Danišík, M., Schmitt, A., Freundt, A. and Pérez, W.: A history of violence: magma incubation, timing, and tephra distribution of the Los Chocoyos super-eruption (Atitlán Caldera, Guatemala), to be submitted.

Clement, A. C., Seager, R., Cane, M. A. and Zebiak, S. E.: An ocean dynamical thermostat, J. Clim., 9(9), 2190–2196, doi:10.1175/1520-0442(1996)009<2190:AODT>2.0.CO;2, 1996.

490   Danabasoglu, G., Lamarque, J.-F., Bacmeister, J., Bailey, D. A., DuVivier, A. K., Edwards, J., Emmons, L., Fasullo, J., Garcia, R., Gettelman, A., Hannay, C., Holland, M. M., Large, W. G., Lawrence, D., Lenaerts, J., Lindsay, K., Lipscomb, W., Lofverstrom, M., Mills, M. J., Neale, R., Oleson, K., Otto-Bleisner, B., Phillips, A., Sacks, W., Tilmes, S., Vertenstein, M., Bertini, A., Deser, C., Fox-Kemper, B., Kay, J. E., Kushner, P., Long, M. C., Mickelson, S., Moore, J. K., Nienhouse, E., Polvani, L., Rasch, P. J., Strand, W. G.: The Community Earth System Model version 2 (CESM2), to be submitted.

495   Drexler, J. W., Rose, W. I., Sparks, R. S. J. and Ledbetter, M. T.: The Los Chocoyos Ash, guatemala: A major stratigraphic marker in middle America and in three ocean basins, Quat. Res., 13(3), 327–345, doi:10.1016/0033-5894(80)90061-7, 1980.

Emile-Geay, J., Seager, R., Cane, M. A., Cook, E. R. and Haug, G. H.: Volcanoes and ENSO over the past millennium, J. Clim., 21(13), 3134–3148, doi:10.1175/2007JCLI1884.1, 2008.

English, J. M., Toon, O. B. and Mills, M. J.: Microphysical simulations of large volcanic eruptions: Pinatubo and Toba, J. Geophys. Res. Atmos., 118(4), 1880–1895, doi:10.1002/jgrd.50196, 2013.

Fisher, R. A., Wieder, W. R., Sanderson, B. M., Koven, C. D., Oleson, K. W., Xu, C., Fisher, J. B., Shi, M., Walker, A. P. and Lawrence, D. M.: Parametric Controls on Vegetation Responses to Biogeochemical Forcing in the CLM5, J. Adv. Model. Earth Syst., 2019MS001609, doi:10.1029/2019MS001609, 2019.

Gettelman, A., Mills, M. J., Kinnison, D. E., Garcia, R. R., Smith, A.K., Marsh, D.R., Tilmes, S., Vitt, F., Bardeen, C. G., McInerny, J. Liu, H.-L., Solomon, S. C., Polvani, L. M., Emmons, L. K., Lamarque, J.-F., Richter, J. H., Glanville, A. S., Bacmeister, J. T., Phillips, A. S., Neale, R. B., Simpson, I. R., DuVivier, A. K., Hodzic, A., Randel, W. J.: The Whole Atmosphere Community Climate Model Version 6 (WACCM6), submitted to J. Geophys. Res. Atmos.

von Glasow, R., Bobrowski, N. and Kern, C.: The effects of volcanic eruptions on atmospheric chemistry, Chem. Geol., 263(1–4), 131–142, doi:10.1016/j.chemgeo.2008.08.020, 2009.

Handler, P.: Possible association of stratospheric aerosols and El Nino type events, Geophys. Res. Lett., 11(11), 1121–1124, doi:10.1029/GL011i011p01121, 1984.

Haslam, M. and Petraglia, M.: Comment on "Environmental impact of the 73ka Toba super-eruption in South Asia" by M.A.J. Williams, S.H. Ambrose, S. van der Kaars, C. Ruehlemann, U. Chattopadhyaya, J. Pal and P.R. Chauhan [Palaeogeography, Palaeoclimatology, Palaeoecology 284 (2009) 295, Palaeogeogr. Palaeoclimatol. Palaeoecol., 296(1–2), 199–203, doi:10.1016/j.palaeo.2010.03.057, 2010.

Iles, C. E., Hegerl, G. C., Schurer, A. P. and Zhang, X.: The effect of volcanic eruptions on global precipitation, J. Geophys. Res. Atmos., 118(16), 8770–8786, doi:10.1002/jgrd.50678, 2013.

Jones, G. S., Gregory, J. M., Stott, P. A., Tett, S. F. B. and Thorpe, R. B.: An AOGCM simulation of the climate response to a volcanic super-eruption, Clim. Dyn., 25(7–8), 725–738, doi:10.1007/s00382-005-0066-8, 2005.

Khodri, M., Izumo, T., Vialard, J., Janicot, S., Cassou, C., Lengaigne, M., Mignot, J., Gastineau, G., Guilyardi, E., Lebas, N., Robock, A. and McPhaden, M. J.: Tropical explosive volcanic eruptions can trigger El Niñõ by cooling tropical Africa, Nat. Commun., 8(1), 778, doi:10.1038/s41467-017-00755-6, 2017.

Klobas, J. E., Wilmouth, D. M., Weisenstein, D. K., Anderson, J. G. and Salawitch, R. J.: Ozone depletion following future volcanic eruptions, Geophys. Res. Lett., 44(14), 7490–7499, doi:10.1002/2017GL073972, 2017.

Krüger, K., Kutterolf, S. and Hansteen, T. H.: Halogen release from Plinian eruptions and depletion of stratospheric ozone, in Volcanism and Global Environmental Change, edited by A. Schmidt, K. E. Fristad, and L. T. Elkins-Tanton, pp. 244–259, Cambridge University Press, Cambridge., 2015.

Kutterolf, S., Hansteen, T. H., Appel, K., Freundt, A., Kruger, K., Perez, W. and Wehrmann, H.: Combined bromine and chlorine release from large explosive volcanic eruptions: A threat to stratospheric ozone?, Geology, 41(6), 707–710, doi:10.1130/G34044.1, 2013.

Kutterolf, S., Hansteen, T. H., Freundt, A., Wehrmann, H., Appel, K., Krüger, K. and Pérez, W.: Bromine and chlorine emissions from Plinian eruptions along the Central American Volcanic Arc: From source to atmosphere, Earth Planet. Sci. Lett., 429, 234–246, doi:10.1016/j.epsl.2015.07.064, 2015.

Kutterolf, S., Schindlbeck, J. C., Anselmetti, F. S., Ariztegui, D., Brenner, M., Curtis, J., Schmid, D., Hodell, D. A., Mueller,
535   A., Pérez, L., Pérez, W., Schwalb, A., Frische, M. and Wang, K.-L.: A 400-ka tephrochronological framework for Central America from Lake Petén Itzá (Guatemala) sediments, Quat. Sci. Rev., 150, 200–220, doi:10.1016/J.QUASCIREV.2016.08.023, 2016.

Li, J., Xie, S. P., Cook, E. R., Morales, M. S., Christie, D. A., Johnson, N. C., Chen, F., D'Arrigo, R., Fowler, A. M., Gou, X. and Fang, K.: El Niño modulations over the past seven centuries, Nat. Clim. Chang., 3(9), 822–826,
540   doi:10.1038/nclimate1936, 2013.

Liu, X., Ma, P.-L., Wang, H., Tilmes, S., Singh, B., Easter, R. C., Ghan, S. J. and Rasch, P. J.: Description and evaluation of a new four-mode version of the Modal Aerosol Module (MAM4) within version 5.3 of the Community Atmosphere Model, Geosci. Model Dev., 9(2), 505–522, doi:10.5194/gmd-9-505-2016, 2016.

Madronich, S. and Flocke, S.: Theoretical Estimation of Biologically Effective UV Radiation at the Earth's Surface, in Solar
545   Ultraviolet Radiation, edited by C. S. Zerefos and A. F. Bais, pp. 23–48, Springer Berlin Heidelberg, Berlin, Heidelberg., 1997.

Metzner, D., Kutterolf, S., Toohey, M., Timmreck, C., Niemeier, U., Freundt, A. and Krüger, K.: Radiative forcing and climate impact resulting from SO2 injections based on a 200,000-year record of Plinian eruptions along the Central American Volcanic Arc, Int. J. Earth Sci., 103(7), 2063–2079, doi:10.1007/s00531-012-0814-z, 2014.

550   Miller, G. H., Geirsdóttir, Á., Zhong, Y., Larsen, D. J., Otto-Bliesner, B. L., Holland, M. M., Bailey, D. A., Refsnider, K. A., Lehman, S. J., Southon, J. R., Anderson, C., Björnsson, H. and Thordarson, T.: Abrupt onset of the Little Ice Age triggered by volcanism and sustained by sea-ice/ocean feedbacks, Geophys. Res. Lett., 39(2), doi:10.1029/2011GL050168, 2012.

Mills, M. J., Schmidt, A., Easter, R., Solomon, S., Kinnison, D. E., Ghan, S. J., Neely, R. R., Marsh, D. R., Conley, A., Bardeen, C. G. and Gettelman, A.: Global volcanic aerosol properties derived from emissions, 1990-2014, using
555   CESM1(WACCM), J. Geophys. Res. Atmos., 121(5), 2332–2348, doi:10.1002/2015JD024290, 2016.

Mills, M. J., Richter, J. H., Tilmes, S., Kravitz, B., MacMartin, D. G., Glanville, A. A., Tribbia, J. J., Lamarque, J.-F., Vitt, F., Schmidt, A., Gettelman, A., Hannay, C., Bacmeister, J. T. and Kinnison, D. E.: Radiative and Chemical Response to Interactive Stratospheric Sulfate Aerosols in Fully Coupled CESM1(WACCM), J. Geophys. Res. Atmos., 122(23), 13,061-13,078, doi:10.1002/2017JD027006, 2017.

560   Muthers, S., Arfeuille, F., Raible, C. C. and Rozanov, E.: The impact of volcanic aerosols on stratospheric ozone and the Northern Hemisphere polar vortex: separating radiative from chemical effects under different climate conditions, Atmos. Chem. Phys. Discuss., 15(10), 14275–14314, doi:10.5194/acpd-15-14275-2015, 2015.

Myhre, G., Shindell, D., Bréon, F.-M., Collins, W. D., Fuglestvedt, J., Huang, J., Koch, D., Lamarque, J.-F., Lee, D., Mendoza, B., Nakajima, T., Robock, A., Stephens, G., Takemura, T. and Zhan, H.: Anthropogenic and natural radiative

565   forcing, in Climate Change 2013 the Physical Science Basis: Working Group I Contribution to the Fifth Assessment Report of the Intergovernmental Panel on Climate Change, vol. 9781107057, edited by Intergovernmental Panel on Climate Change, pp. 659–740, Cambridge University Press, Cambridge., 2013.

Niemeier, U., Timmreck, C. and Krüger, K.: Revisiting the Agung 1963 volcanic forcing – impact of one or two eruptions, Atmos. Chem. Phys. Discuss., 1–18, doi:10.5194/acp-2019-415, 2019.

570   Ohba, M., Shiogama, H., Yokohata, T. and Watanabe, M.: Impact of Strong Tropical Volcanic Eruptions on ENSO Simulated in a Coupled GCM, J. Clim., 26(14), 5169–5182, doi:10.1175/JCLI-D-12-00471.1, 2013.

Pinto, J. P., Turco, R. P. and Toon, O. B.: Self-limiting physical and chemical effects in volcanic eruption clouds, J. Geophys. Res., 94(D8), 11165, doi:10.1029/JD094iD08p11165, 1989.

Plumb, R. A.: Stratospheric Transport, J. Meteorol. Soc. Japan. Ser. II, 80(4B), 793–809, doi:10.2151/jmsj.80.793, 2002.

575   Rampino, M. R. and Self, S.: Volcanic winter and accelerated glaciation following the Toba super-eruption, Nature, 359(6390), 50–52, doi:10.1038/359050a0, 1992.

Rampino, M. R. and Self, S.: Climate-volcanism feedback and the toba eruption of ∼74,000 years ago, Quat. Res., 40(3), 269–280, doi:10.1006/qres.1993.1081, 1993.

Robock, A.: Volcanic eruptions and climate, Rev. Geophys., 38(2), 191–219, doi:10.1029/1998RG000054, 2000.

580   Robock, A. and Liu, Y.: The Volcanic Signal in Goddard Institute for Space Studies Three-Dimensional Model Simulations, J. Clim., 7(1), 44–55, doi:10.1175/1520-0442(1994)007<0044:TVSIGI>2.0.CO;2, 1994.

Robock, A., Ammann, C. M., Oman, L., Shindell, D., Levis, S. and Stenchikov, G.: Did the Toba volcanic eruption of ∼74 ka B.P. produce widespread glaciation?, J. Geophys. Res. Atmos., 114(10), D10107, doi:10.1029/2008JD011652, 2009.

Seinfeld, J. H. and Pandis, S. N.: Atmospheric chemistry and physics: from air pollution to climate change, John Wiley & 585   Sons., 2016.

Solomon, S.: Stratospheric ozone depletion: A review of concepts and history, Rev. Geophys., 37(3), 275, doi:10.1029/1999RG900008, 1999.

Stenchikov, G., Delworth, T. L., Ramaswamy, V., Stouffer, R. J., Wittenberg, A. and Zeng, F.: Volcanic signals in oceans, J. Geophys. Res., 114(D16), D16104, doi:10.1029/2008JD011673, 2009.

590   Stevenson, S., Otto-Bliesner, B., Fasullo, J. and Brady, E.: "El Niño Like" hydroclimate responses to last millennium volcanic eruptions, J. Clim., 29(8), 2907–2921, doi:10.1175/JCLI-D-15-0239.1, 2016.

Stevenson, S., Fasullo, J. T., Otto-Bliesner, B. L., Tomas, R. A. and Gao, C.: Role of eruption season in reconciling model and proxy responses to tropical volcanism, Proc. Natl. Acad. Sci., 114(8), 1822–1826, doi:10.1073/pnas.1612505114, 2017.

Svensson, A., Bigler, M., Blunier, T., Clausen, H. B., Dahl-Jensen, D., Fischer, H., Fujita, S., Goto-Azuma, K., Johnsen, S. 595   J., Kawamura, K., Kipfstuhl, S., Kohno, M., Parrenin, F., Popp, T., Rasmussen, S. O., Schwander, J., Seierstad, I., Severi, M., Steffensen, J. P., Udisti, R., Uemura, R., Vallelonga, P., Vinther, B. M., Wegner, A., Wilhelms, F. and Winstrup, M.: Direct linking of Greenland and Antarctic ice cores at the Toba eruption (74 ka BP), Clim. Past, 9(2), 749–766, doi:10.5194/cp-9-749-2013, 2013.

Timmreck, C., Graf, H.-F. F. and Steil, B.: Aerosol Chemistry Interactions After the Mt. Pinatubo Eruption, in Volcanism
and the Earth's Atmosphere, vol. 139, pp. 213–225, American Geophysical Union (AGU)., 2003.

Timmreck, C., Graf, H.-F., Lorenz, S. J., Niemeier, U., Zanchettin, D., Matei, D., Jungclaus, J. H. and Crowley, T. J.:
Aerosol size confines climate response to volcanic super-eruptions, Geophys. Res. Lett., 37(24),
doi:10.1029/2010GL045464, 2010.

Timmreck, C., Graf, H. F., Zanchettin, D., Hagemann, S., Kleinen, T. and Krüger, K.: Climate response to the Toba super-
eruption: Regional changes, Quat. Int., 258, 30–44, doi:10.1016/j.quaint.2011.10.008, 2012.

Timmreck, C., Mann, G. W., Aquila, V., Hommel, R., Lee, L. A., Schmidt, A., Brühl, C., Carn, S., Chin, M., Dhomse, S. S.,
Diehl, T., English, J. M., Mills, M. J., Neely, R., Sheng, J., Toohey, M. and Weisenstein, D.: The Interactive Stratospheric
Aerosol Model Intercomparison Project (ISA-MIP): motivation and experimental design, Geosci. Model Dev., 11(7), 2581–
2608, doi:10.5194/gmd-11-2581-2018, 2018.

Toohey, M., Krüger, K. and Timmreck, C.: Volcanic sulfate deposition to Greenland and Antarctica: A modeling sensitivity
study, J. Geophys. Res. Atmos., 118(10), 4788–4800, doi:10.1002/jgrd.50428, 2013.

Vidal, C. M., Métrich, N., Komorowski, J.-C., Pratomo, I., Michel, A., Kartadinata, N., Robert, V. and Lavigne, F.: The
1257 Samalas eruption (Lombok, Indonesia): the single greatest stratospheric gas release of the Common Era, Sci. Rep.,
6(October), 34868, doi:10.1038/srep34868, 2016.

Williams, M. A. J., Ambrose, S. H., van der Kaars, S., Ruehlemann, C., Chattopadhyaya, U., Pal, J. and Chauhan, P. R.:
Environmental impact of the 73 ka Toba super-eruption in South Asia, Palaeogeogr. Palaeoclimatol. Palaeoecol., 284(3–4),
295–314, doi:10.1016/j.palaeo.2009.10.009, 2009.

WMO: Scientific Assessment of Ozone Depletion: 2014, Geneva, Switzerland., 2014.

WMO: Scientific Assessment of Ozone Depletion: 2018, Geneva, Switzerland., 2018.

Zanchettin, D., Timmreck, C., Graf, H. F., Rubino, A., Lorenz, S., Lohmann, K., Krüger, K. and Jungclaus, J. H.: Bi-decadal
variability excited in the coupled ocean-atmosphere system by strong tropical volcanic eruptions, Clim. Dyn., 39(1–2), 419–
444, doi:10.1007/s00382-011-1167-1, 2012.

Zanchettin, D., Khodri, M., Timmreck, C., Toohey, M., Schmidt, A., Gerber, E. P., Hegerl, G., Robock, A., Pausata, F. S. R.,
Ball, W. T., Bauer, S. E., Bekki, S., Dhomse, S. S., LeGrande, A. N., Mann, G. W., Marshall, L., Mills, M., Marchand, M.,
Niemeier, U., Poulain, V., Rozanov, E., Rubino, A., Stenke, A., Tsigaridis, K. and Tummon, F.: The Model Intercomparison
Project on the climatic response to Volcanic forcing (VolMIP): experimental design and forcing input data for CMIP6,
Geosci. Model Dev., 9(8), 2701–2719, doi:10.5194/gmd-9-2701-2016, 2016.

Zhong, Y., Miller, G. H., Otto-Bliesner, B. L., Holland, M. M., Bailey, D. A., Schneider, D. P. and Geirsdottir, A.:
Centennial-scale climate change from decadally-paced explosive volcanism: a coupled sea ice-ocean mechanism, Clim.
Dyn., 37(11–12), 2373–2387, doi:10.1007/s00382-010-0967-z, 2011.

Zielinski, G. A., Mayewski, P. A., Meeker, L. D., Whitlow, S., Twickler, M. S. and Taylor, K.: Potential atmospheric impact
of the Toba mega-eruption ∼71,000 years ago, Geophys. Res. Lett., 23(8), 837–840, doi:10.1029/96GL00706, 1996.

Tables

Ensemble name	Experiment name	Branch year	Initial QBO state at 30 hPa	Initial ENSO state (ONI)	Length [years]	Injected sulfur [Mt]	Injected chlorine [Mt]	Injected bromine [Mt]
CTR	Control run (CTR)	-	-	-	70	-	-	-
LCY_full	LCY_full.qboE.ensoN	13	E	Neutral	35	523	120	0.2
LCY_full	LCY_full.qboE.ensoM	15	E	La Niña	35	523	120	0.2
LCY_full	LCY_full.qboE.ensoP	17	E	El Niño	35	523	120	0.2
LCY_full	LCY_full.qboW.ensoN	30	W	Neutral	35	523	120	0.2
LCY_full	LCY_full.qboW.ensoM	23	W	La Niña	35	523	120	0.2
LCY_full	LCY_full.qboW.ensoP	18	W	El Niño	35	523	120	0.2
LCY_sulf	LCY_sulf.qboE.ensoN	13	E	Neutral	35	523	0	0
LCY_sulf	LCY_sulf.qboW.ensoN	30	W	Neutral	35	523	0	0
LCY_1%sulf	LCY_1%sulf.qboE.ensoN	13	E	Neutral	10	5.23	0	0
LCY_1%halog	LCY_1%halog.qboE.ensoN	13	E	Neutral	35	523	12	0.02

635 **Table 1: Summary of model experiments. The injected volatile mass to the stratosphere is based on the total erupted masses of 523 Mt sulfur, 1200 Mt chlorine and 2 Mt bromine applying different injection efficiencies (see Experiment names and Section Methods)**

640

Figures
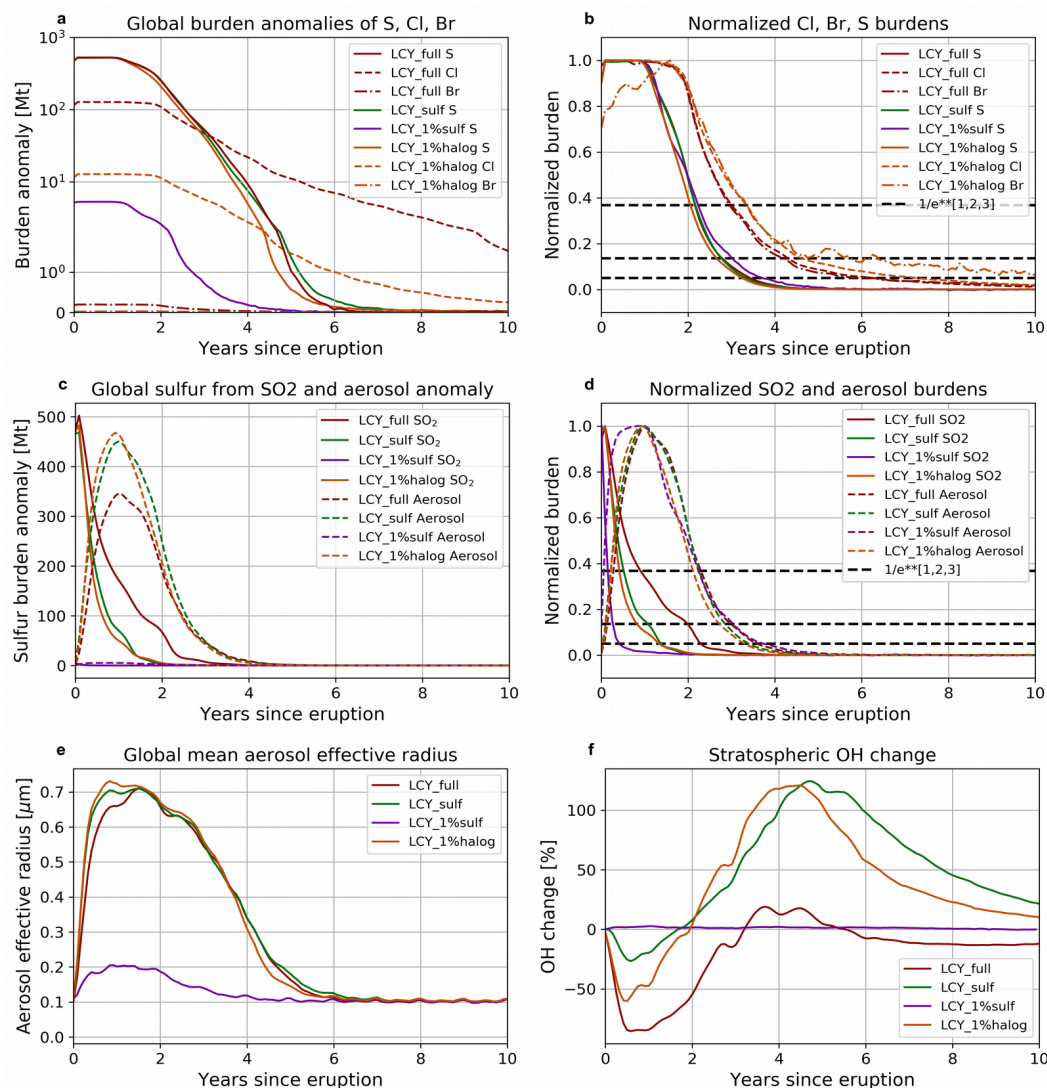
Figure 1: Global evolution of sulfur, halogens, aerosols and OH for the Los Chocoyos simulations. (a) Total sulfur and halogen burden anomalies. (b) Normalized sulfur and halogen burdens. Dashed horizontal lines represents 1/e, 1/e2 and 1/e3. (c) SO₂ and sulfate aerosols burdens. (d) Same as (b) but for SO₂ and sulfate aerosol burdens. (e) Global mean aerosol effective radius. (f) Time evolution of OH change relative to CTR. Dashed horizontal lines in b) and d) represents 1/e, 1/e² and 1/e³.

645
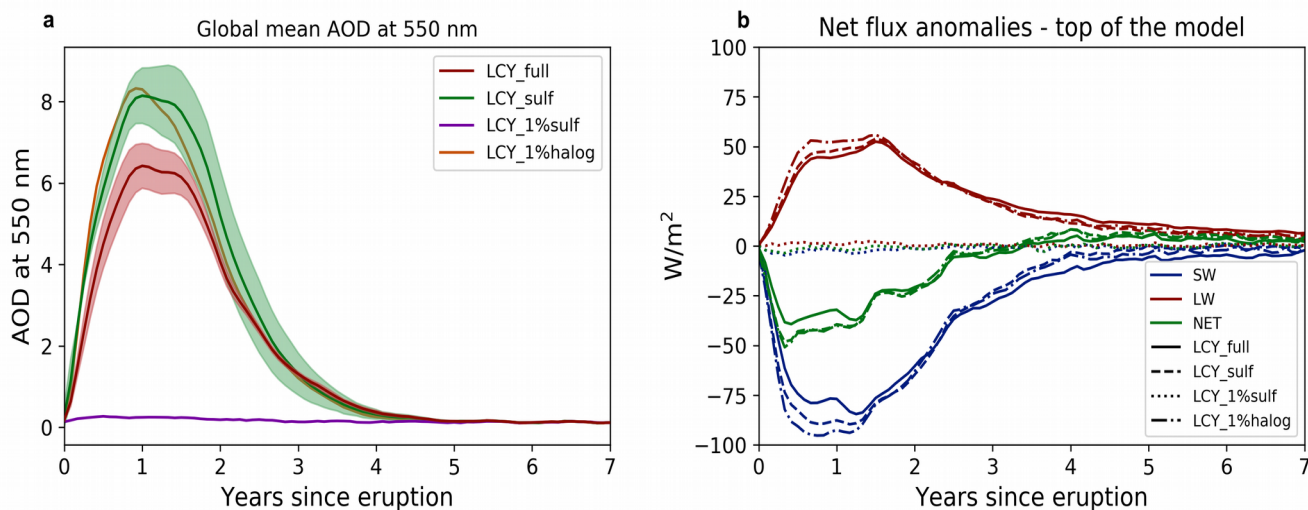
Figure 2: Total aerosol optical depth (AOD) at 550 nm and net radiative flux anomalies at the top of the model in the four LCY eruption scenarios.
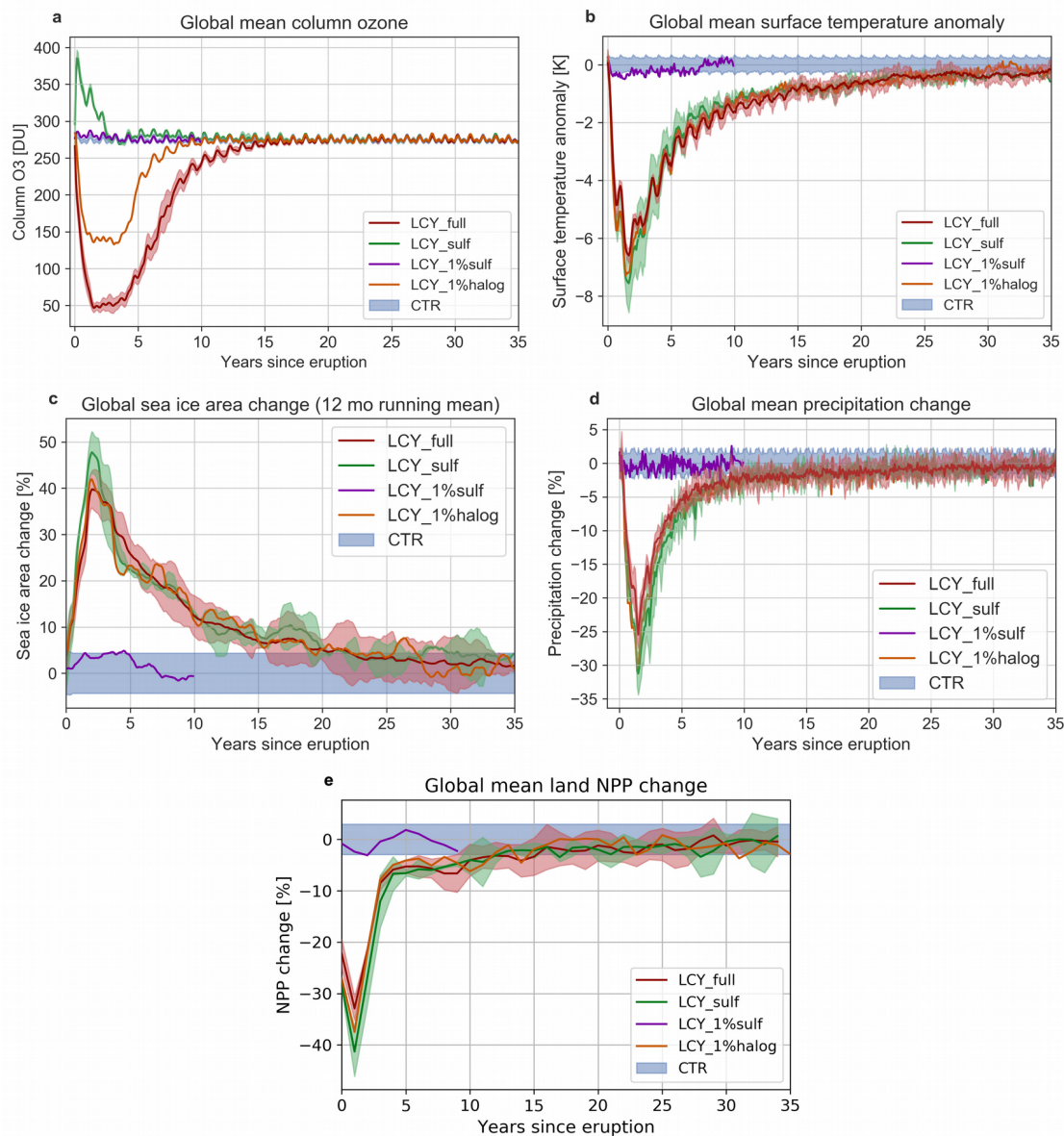
Figure 3: Global mean time-series of column ozone (a) surface temperature anomalies (b), sea ice area change (c), precipitation
650 **change (d) and annual mean NPP change (e) in the LCY simulation scenarios.**
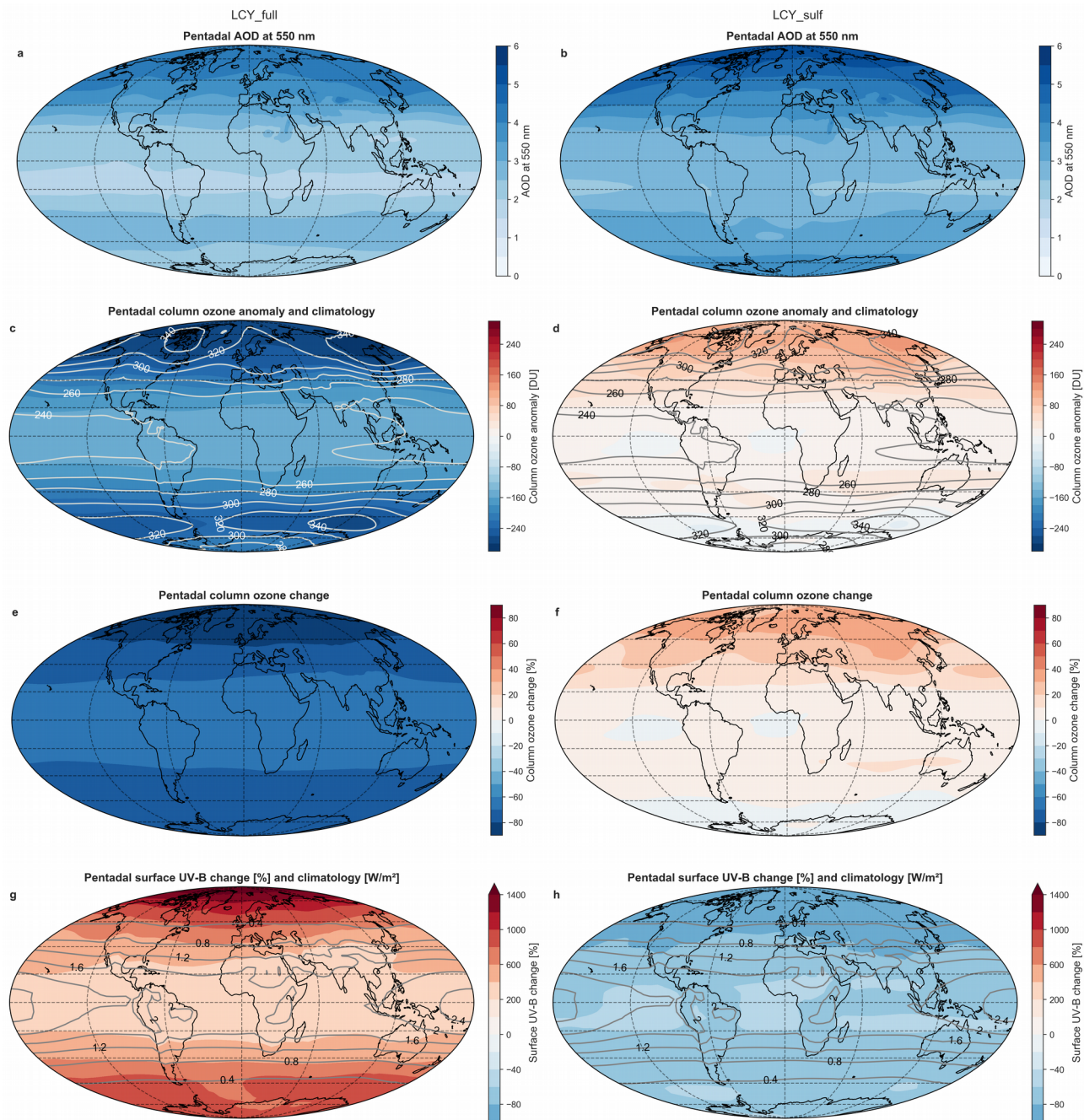
Figure 4: Maps of post-eruption pentadal mean AOD (a,b), ozone anomaly and climatology (c,d), ozone change (e,f) and surface UV-B weighted for DNA damage change and climatology (g,h) for left side LCY_full (a,c,e,g) and right side LCY_sulf (b,d,f,h).
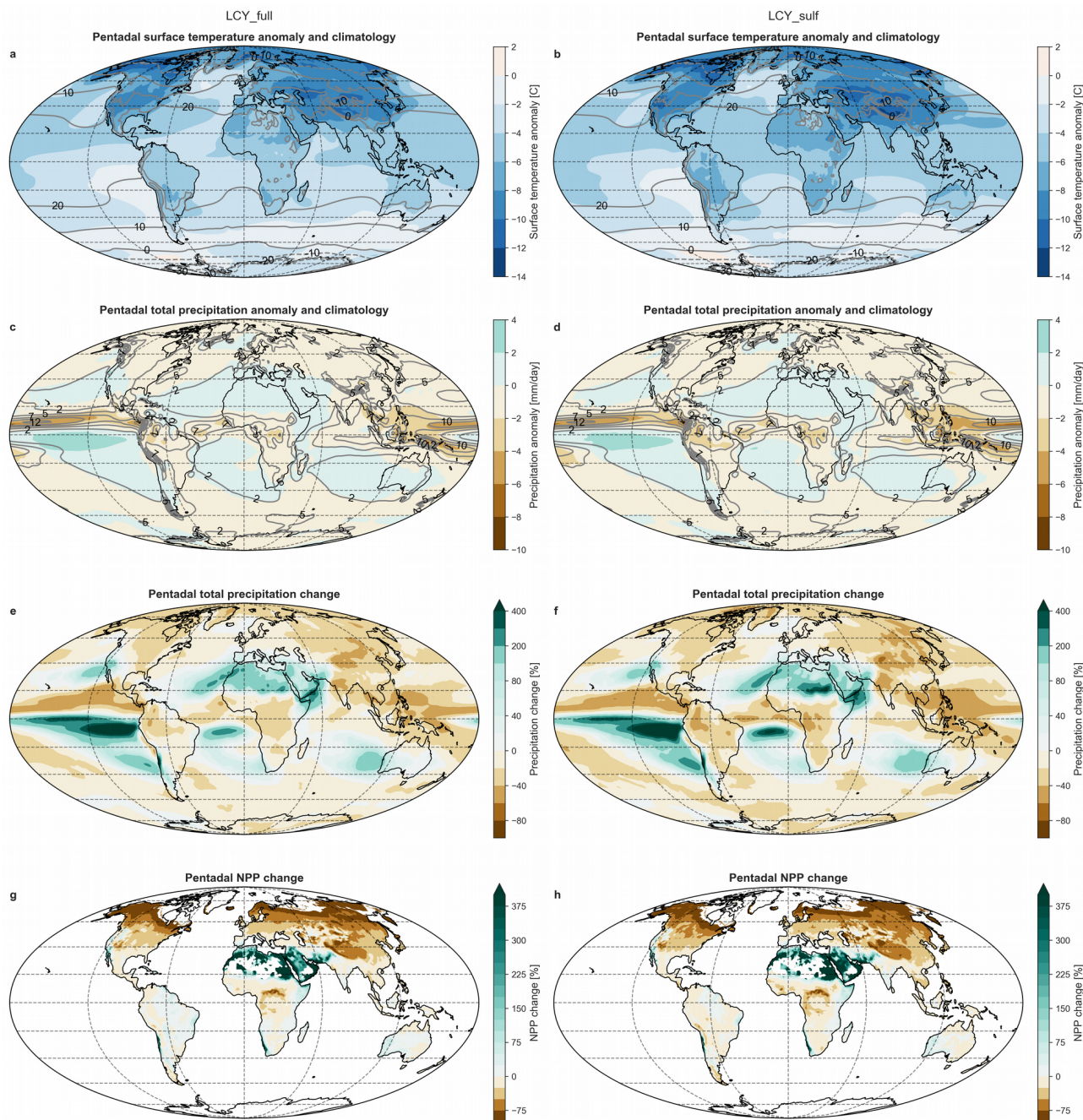
Figure 5: Maps of post-eruption pentadal mean surface temperature anomaly and climatology (a,b), precipitation anomaly and climatology (c,d), precipitation change (e,f) and NPP change (g,h) for LCY_full (left side: a,c,e,g) and LCY_sulf (right side: b,d,f,h). White areas on the NPP maps indicates invalid values.
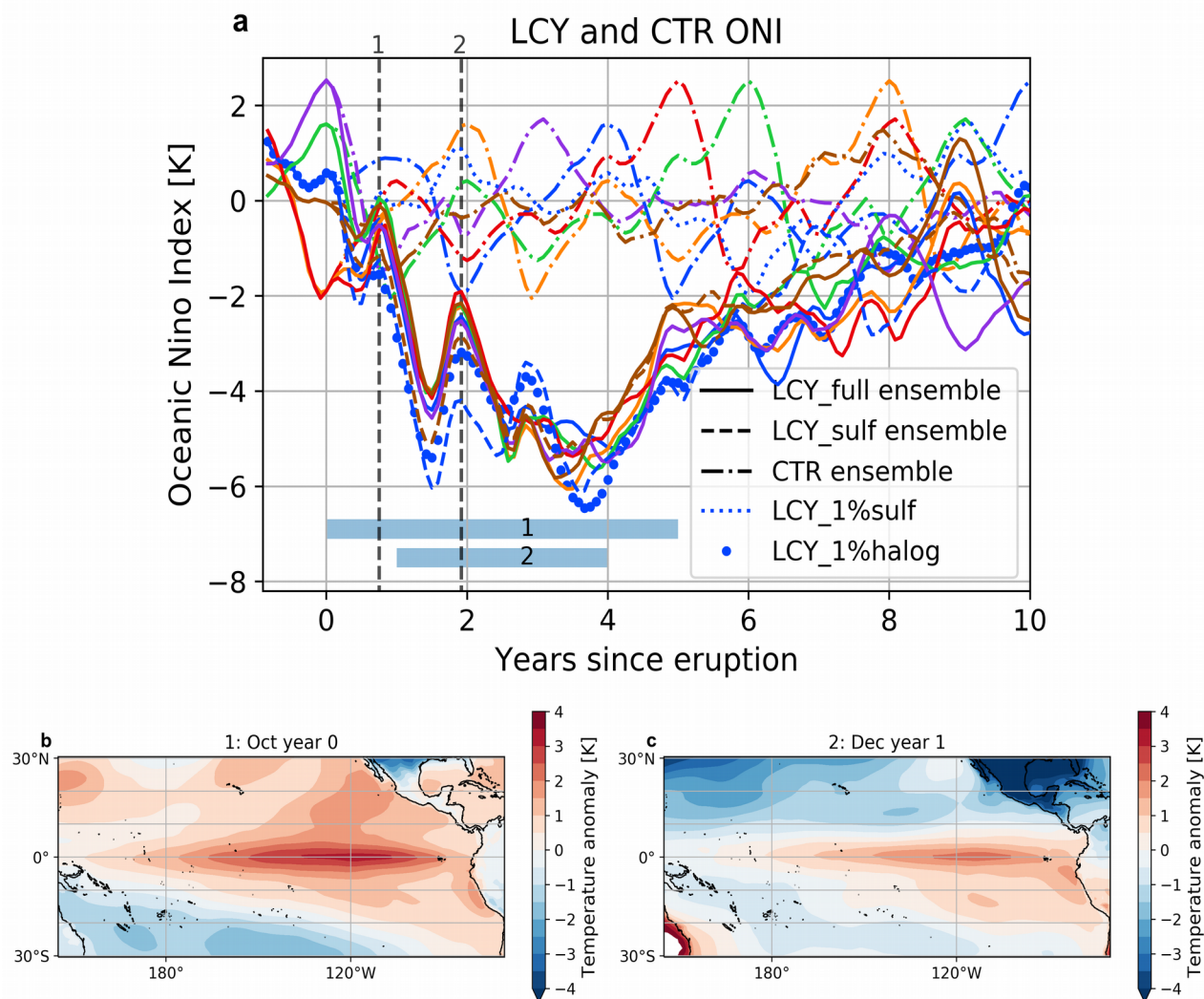
Figure 6: ENSO response to the simulated Los Chocoyos eruption and CTR. (a) ONI time series for the LCY_full ensemble, LCY_sulf and LCY_1%sulf and for the corresponding ensemble without eruption constructed from the control simulation. SST maps for the equatorial Pacific showing the maximum response to the LCY_full forcing scenario during b) October of year 0 and c) December of year 1. The baselines for the two anomalies are indicated by the box in (a).
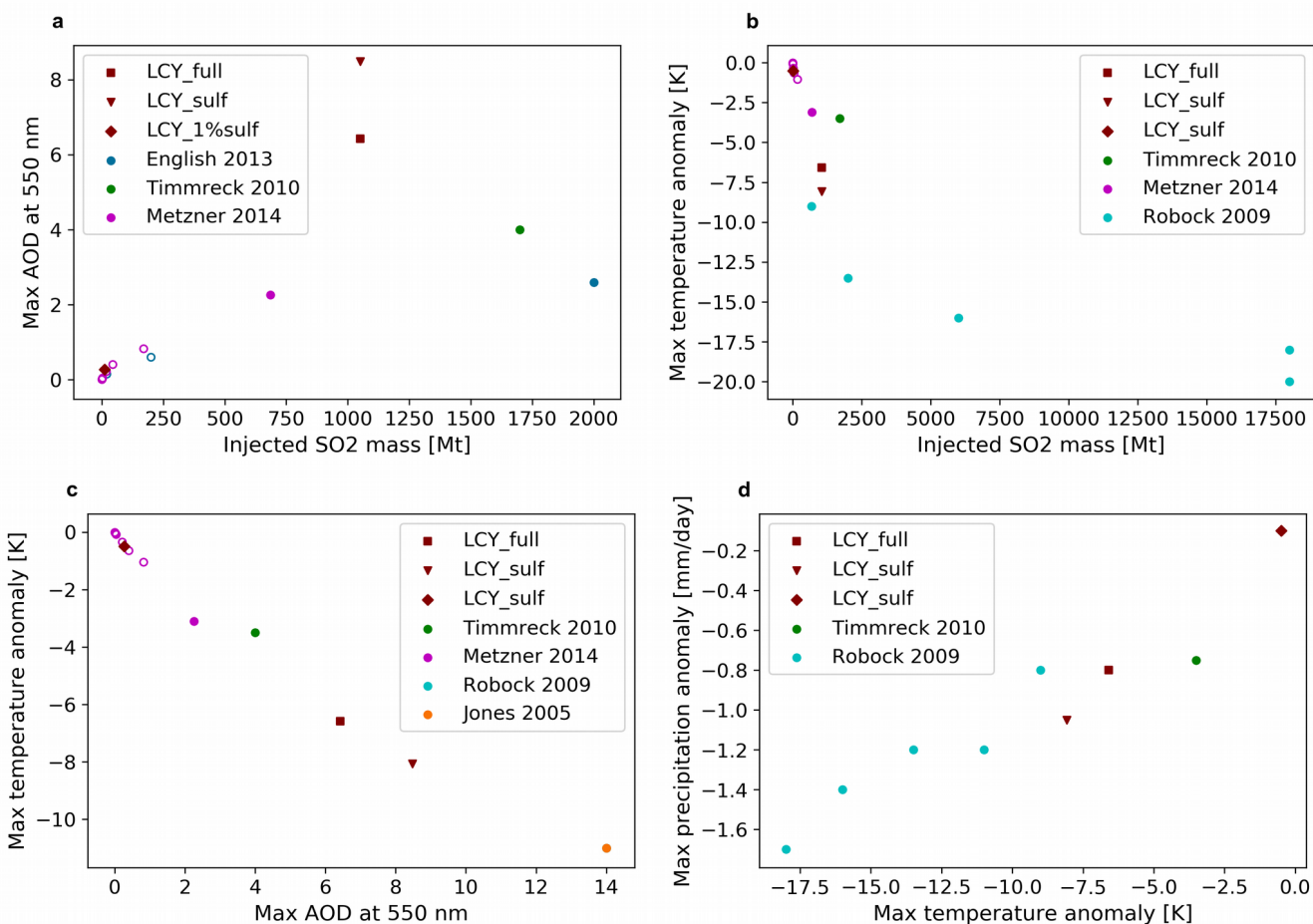
660 **Figure 7: Scatter plots comparing our Los Chocoyos simulations to other super-size volcanic eruption simulations from Jones et al. (2005), Robock et al. (2009), Timmreck et al. (2010), English et al. (2013) and Metzner et al. (2014). Large to extremely large explosive eruptions not classified as super-eruptions are marked with open circles.**